Brain Extraction Using Geodesic Active Contours

Albert Huang*[a], Rafeef Abugharbieh[a], Roger Tam[b], Anthony Traboulsee[b]

[a]Dept. of Elect. & Comp. Eng., University of British Columbia, Vancouver, BC, V6T 1Z4, Canada
[b]Dept. of Medicine, University of British Columbia, Vancouver, BC, V6T 1Z3, Canada

ABSTRACT

Extracting the brain cortex from magnetic resonance imaging (MRI) head scans is an essential preprocessing step of which the accuracy greatly affects subsequent image analysis. The currently popular Brain Extraction Tool (BET) produces a brain mask which may be too smooth for practical use. This paper presents a novel brain extraction tool based on three-dimensional geodesic active contours, connected component analysis and mathematical morphology. Based on user-specified intensity and contrast levels, the proposed algorithm allows an active contour to evolve naturally and extract the brain cortex. Experiments on synthetic MRI data and scanned coronal and axial MRI image volumes indicate successful extraction of tight perimeters surrounding the brain cortex. Quantitative evaluations on both synthetic phantoms and manually labeled data resulted in better accuracy than BET in terms of true and false voxel assignment. Based on these results, we illustrate that our brain extraction tool is a robust and accurate approach for the challenging task of automatically extracting the brain cortex in MRI data.

Keywords: Segmentation, geodesic active contours, mathematical morphology, magnetic resonance imaging (MRI), neuroimaging, Multiple Sclerosis (MS).

1. INTRODUCTION

Extracting the brain cortex from magnetic resonance imaging (MRI) head scans is one of the important pre-processing steps in analyzing intracranial volumes. Any subsequent analysis, such as tissue segmentation or brain volume and atrophy measurement, will be highly dependent on the robustness and precision of the brain masks generated in the brain extraction step. By accurately defining the brain cortex, one could essentially minimize errors for the analyses that follow.

A number of techniques have been proposed for brain mask extraction from MRI data. A tessellated deformable sphere model has been used by Smith *et al* [1] and is implemented in the popular Brain Extraction Tool (BET). BET performs well on synthetic data; however, results are poor and inconsistent when applied to real MRI scans (as observed in Section 4). Shattuck *et al* [2] developed a Brain Surface Extraction algorithm (BSE) based on mathematical morphology and connected component operations; however, BSE masks are often too smooth for standalone application as described in his paper. Lemieux *et al* [3] used thresholding, Gaussian fitting, and connected component operations for this task but their technique has only been tested on synthetic data. Rehm *et al* [4] offered a different approach by generating a consensus mask from an atlas-registered mask, a histogram-based mask and a BSE mask but the tool dependency and setup is too complex for practical use.

Our proposed method pre-processes MRI scans to generate inputs to a deformable model, namely a geodesic active contour. After the model converges to a stable solution, the mask is post-processed to further refine the perimeter of the brain cortex. The pre-processing and post-processing stages employ the Otsu's thresholding method [5] based on a mixture of Gaussian models assumption, as well as mathematical morphology and connected component analysis. The algorithm in this paper focuses on T1-weighted scans; work is under way to extend the method to other MR modalities.

Medical Imaging 2006: Image Processing, edited by Joseph M. Reinhardt, Josien P. W. Pluim,
Proc. of SPIE Vol. 6144, 61444J, (2006) · 0277-786X/06/$15 · doi: 10.1117/12.654160

2. METHODOLOGY

Our brain extraction algorithm starts by correcting for existing bias fields and noise artifacts. We apply the N3 bias field correction tool [6] and a Perona-Malik anisotropic diffusion filter [7] to our data before proceeding with the cortex extraction algorithm.

2.1. Review of geodesic active contours

The geodesic active contours [8] framework transforms the energy minimization problem of an energy-based deformable model into finding the geodesic or the minimal distance curve in a Riemannian space by using a gradient descent search and the Euler-Lagrange equation. An initial curve C_0 is deformed according to the curve evolution equation:

$$\frac{\partial C}{\partial t} = g(I)(c+\kappa)\vec{N} - (\nabla g \cdot \vec{N})\vec{N} \qquad (1)$$

where κ is the Euclidean curvature, $\vec{N}$ is the inner unit normal, g is some general function of the intensity I, c is a constant velocity term acting as a balloon force, and $\partial C/\partial t = \kappa\vec{N}$ is the Euclidean heat flow equation satisfying the geometric smoothing property [8].

Equation (1) can be embedded in a level-set of a function u as in (2), and then one searches for the steady state solution.

$$\frac{\partial u}{\partial t} = g|\nabla u|(c+\kappa) + \nabla g \cdot \nabla u \qquad (2)$$

The general function g acts as a feature function for determining the evolution and halting speed of the evolving curve, where a value of zero represents an ideal edge. Section 2.2.3 describes the feature function g for our proposed method.

2.2. Pre-processing

Before our geodesic active contour could be initialized in MRI scans, several pre-processing steps are necessary to ensure a stable convergence of the contour to the appropriate perimeter.

2.2.1. Tissue removal

Otsu [5] developed a threshold selection criterion by minimizing the interclass variance. We apply this threshold for brain and non-brain separation using a two-Gaussian mixture model. The brain tissue is divided into three intensity ranges, each of which is further divided into three sub-ranges based on additional applications of the Otsu thresholding technique. With user-specified white matter (WM) intensity level ("low", "medium" or "high"), and white and gray matter (GM) contrast ("lowest", "low" or "normal"), two contiguous subsets of these nine intensity ranges are selected, one for initializing the contour and the other for computing the feature image.

2.2.2. Initializing the active contour

The level-set approach requires an initial contour as the zero level-set from which the active contour then propagates. To initialize a suitable contour inside the regions to be segmented, we choose the WM region for initialization since its intensity is the highest in T1-weighted data, therefore providing better separability from the low intensity cerebrospinal fluid (CSF) than GM. The WM intensity range is provided by the user-specified WM intensity level ("low", "medium" or "high") based on visual inspection of the data (see Table 1).

With low WM intensity level, WM is assigned an intensity range at the low end (O_3) but higher than the intensity range assumed to be GM (O_2) and CSF (O_1). With medium WM intensity level, WM is assumed to be closer to the middle of the range (O_4-O_6). The highest range (O_7-O_9) is assumed to be eyes and scalp, whereas the lower range (O_1-O_3) is assumed to be GM and CSF. With high WM intensity level, WM is assumed to be within the higher range (O_7-O_8) with range (O_9) assumed to be high intensity outliers.

The resulting tissue mask is further eroded with a 3D spherical structural element of a 1-voxel radius to remove edge regions that might have partial volume effects with the adjacent tissues. Pruning and connected component operations are then performed to ensure the initial contour is the largest connected component.

2.2.3. Feature image

The feature image from which the active contour derives its speed term and stopping function should be established based on a combined estimate of GM and WM. Based on user-specified WM/GM contrast level ("lowest", "low" or "normal"), we extend our data range from the initial contour range to further include GM (see Table 1). A Gaussian smoothing is then used with 3mm variance to allow fuzzy edges for the contour evolution but without linking the desired anatomic brain region to other non-brain areas.

Table 1. Tissue intensity ranges for geodesic active contours.

User-Specified Values		Intensity Range		
Intensity	Contrast	*Range of Interests*	*Initial Contour*	*Feature Image*
1 (Low)	*1/2/3 (---)*	$O_1 \sim O_3$	O_3	$O_2 \sim O_3$
2 (Medium)	*1 (Lowest)*	$O_1 \sim O_6$	$O_4 \sim O_6$	$O_4 \sim O_6$
	2 (Low)	$O_1 \sim O_6$	$O_4 \sim O_6$	$O_3 \sim O_6$
	3 (Normal)	$O_1 \sim O_6$	$O_4 \sim O_6$	$O_2 \sim O_6$
3 (High)	*1 (Lowest)*	$O_1 \sim O_9$	$O_7 \sim O_8$	$O_7 \sim O_8$
	2 (Low)	$O_1 \sim O_9$	$O_7 \sim O_8$	$O_6 \sim O_8$
	3 (Normal)	$O_1 \sim O_9$	$O_7 \sim O_8$	$O_4 \sim O_8$

Note: O_m indicates the m^{th} intensity range determined by the tissue removal step.

2.3. Post-processing

After the geodesic active contour converges to a stable solution, the largest connected component is determined before further refinement is applied.

2.3.1. Morphological dilation

The mask resulting from the active contour is dilated with a 3D spherical structural element of a 2-voxel radius to expand its coverage in order to compensate for our conservative model feature image described in Section 2.2.3, and the resulting contour.

2.3.2. Hole-closing operation

A morphological opening operation is applied with a 1-voxel radius spherical structural element to untie any falsely linked tissues. Hole-closing is then performed in the axial, coronal and sagittal directions by finding the largest connected component in the background and filling those background pixels which do not belong to the largest connected background component.

3. DATA

For the simulated data tested, we used 18 synthetic volumes from the BrainWeb simulated brain database [9-12]. The T1-weighted modality data and the provided phantom are 1mm×1mm×1mm in spacing. Noise level varies at 0%, 1%, 3%, 5%, 7% and 9%, and intensity non-uniformity varies at 0%, 20% and 40%.

The 20 normal MR brain data sets and their manual segmentations were provided by the Center for Morphometric Analysis at Massachusetts General Hospital and are available at http://www.cma.mgh.harvard.edu/ibsr/. We selected only 10 datasets out of these 20 T1-weighted spoiled gradient echo volumes from the International Brain Segmentation Repository (IBSR) because of severe intensity inhomogeneity problems in the other 10 sets which is not the focus of this study. The data are acquired coronally with 1mm×3.1mm×1mm in spacing.

We also examined 15 clinical T1-weighted axial data from the Multiple Sclerosis MRI Research Group (MS/MRI) at the University of British Columbia with 256×256×50 resolution and 0.937mm×0.937mm×3mm in spacing.

4. RESULTS AND DISCUSSIONS

We evaluated both quantitative and qualitative results on synthetic BrainWeb and real IBSR data. Since no manual segmentation masks existed for the MS/MRI research group data, those were only qualitatively evaluated.

4.1. Quantitative results

On the 18 BrainWeb scans, BET achieves an average of 99.58% sensitivity for WM and GM, and 97.63% specificity for WM, GM and CSF. Our proposed method achieves an average of 99.58% sensitivity for WM and GM, and 98.27% specificity for WM, GM and CSF (see Figure 1). Since the BrainWeb phantom contains CSF surrounding the brain cortex, our sensitivity is calculated based only on GM and WM, whereas specificity is calculated based on GM, WM and CSF.

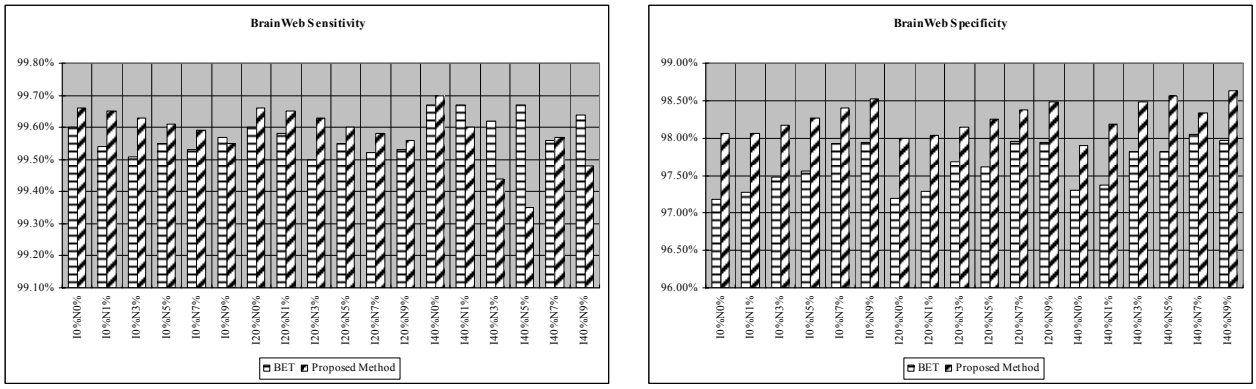

Figure 1. Quantitative comparisons of sensitivity (left) and specificity (right) on BrainWeb scans with BET and our brain extraction method. The horizontal axis label specifies various inhomogeneity (I) and noise (N) levels.

On 10 selected IBSR scans with less severe intensity inhomogeneity problem, BET achieves an average of 92.88% similarity index, 15.32% misclassification rate and 14.79% volume difference error, whereas our method achieves an average of 94.53% similarity index, 11.51% misclassification rate and 9.89% volume difference error (see Figure 2).

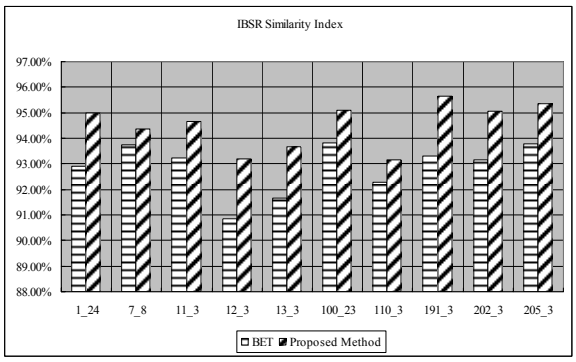

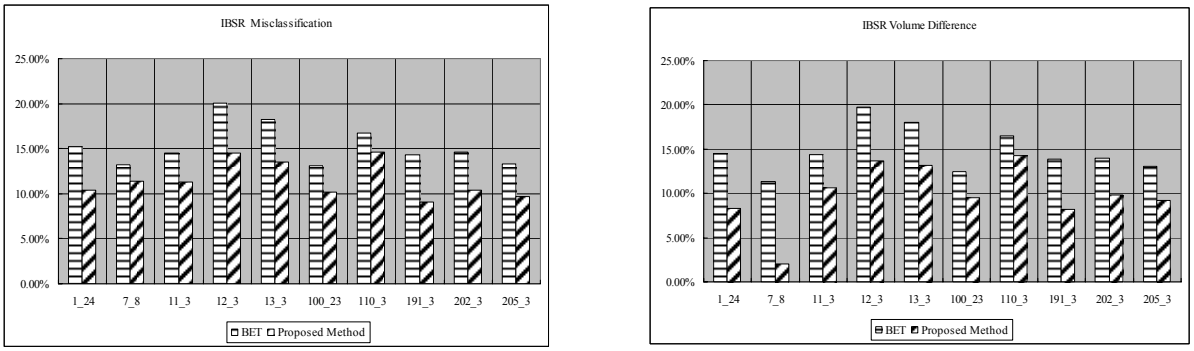

Figure 2. Quantitative comparisons of similarity index (top), misclassification rates (bottom left) and intracranial volume differences (bottom right) on IBSR scans with BET and our brain extraction method.

4.1. Qualitative results

To demonstrate the superior results obtained using our proposed method, we show an example three-dimensional (3D) brain extraction result on BrainWeb data (see Figure 3) which clearly illustrates that our method produces a tighter brain mask than BET.

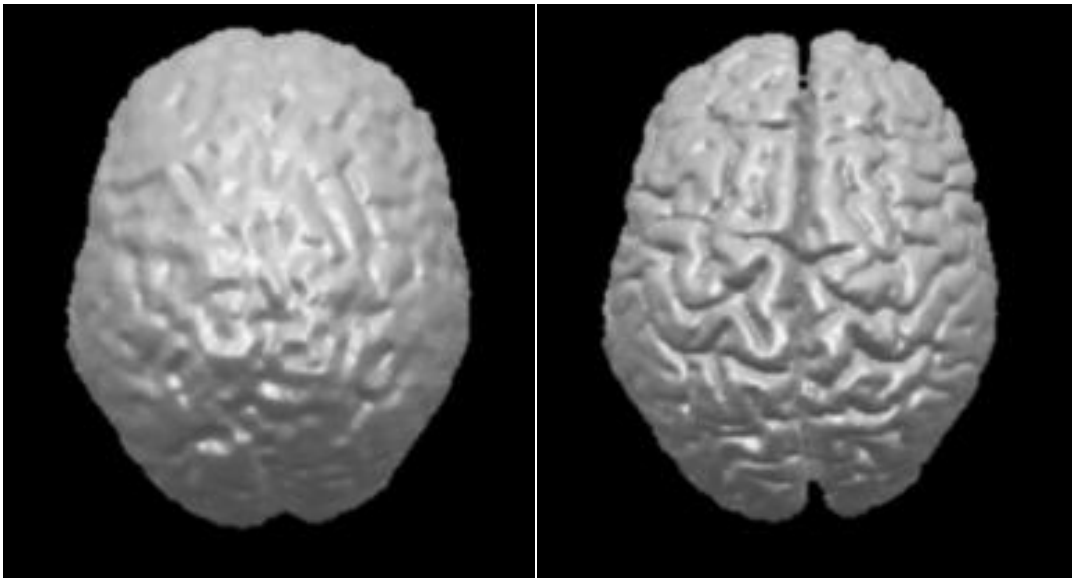

Figure 3. Example 3D rendering of a brain mask obtained using BET (left) as opposed to using our brain extraction method (right) on BrainWeb synthetic T1-weighted data.

Next, we present sample two-dimensional (2D) brain extraction results on BrainWeb scans (see Figure 4), and demonstrate these same differences in brain extraction performance with the highlighted regions.

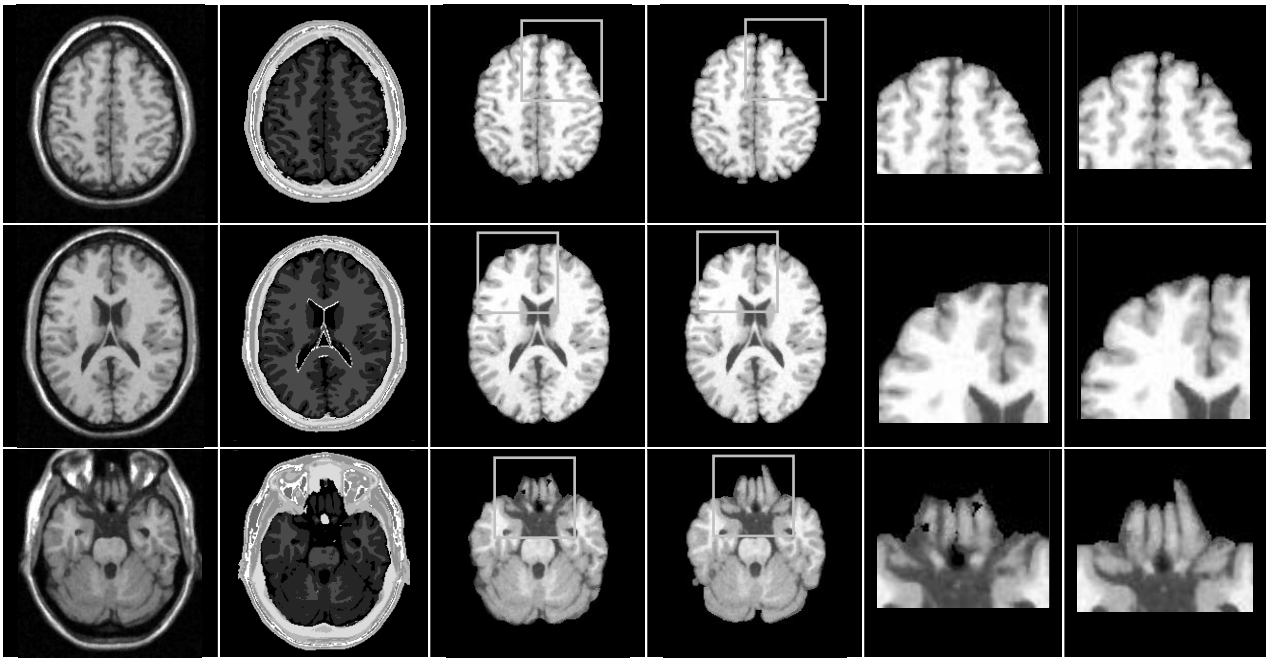

Figure 4. Axial slices (from top to bottom) of a BrainWeb synthetic T1-weighted scan, the BrainWeb phantom, BET results, our brain extraction results, highlighted BET results, and our highlighted brain extraction results (from left to right).

Next we examine the IBSR results (Figure 5) and observe similar findings. The highlighted regions indicate a closer match to the manual segmentations with our proposed method than with BET.

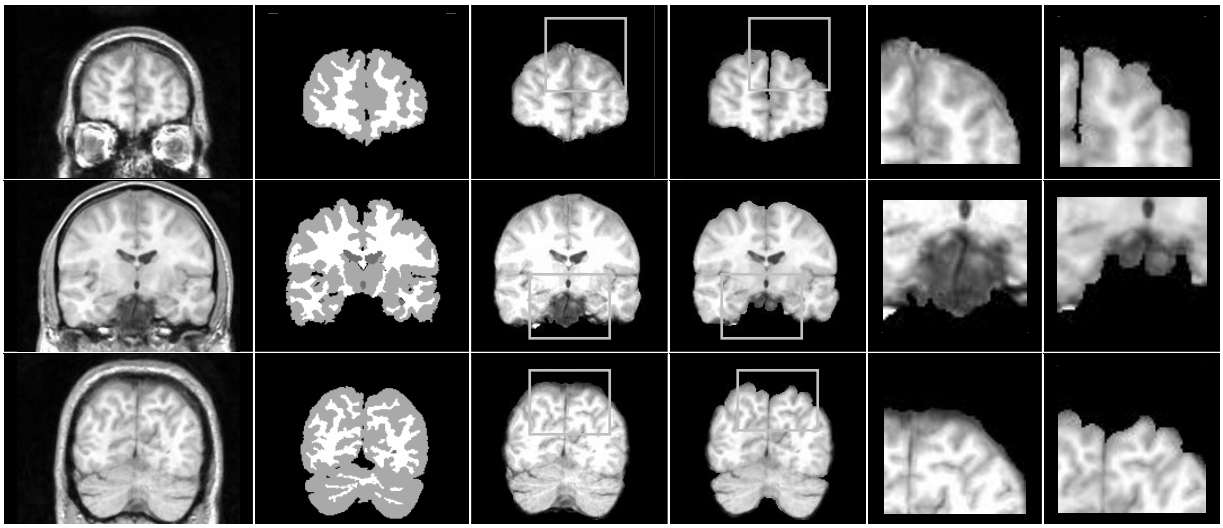

Figure 5. Coronal slices (from top to bottom) of IBSR T1-weighted scan #12_3, manual segmentation results, BET results, our brain extraction results, highlighted BET results, and our highlighted brain extraction results (from left to right).

Lastly, we compare the brain extraction performance when applying to real clinical data from the UBC MS/MRI Research Group (Figure 6) in 3D. Again as seen with the BrainWeb results, the 3D rendering demonstrates that our proposed method produces a superior and tighter brain mask than the one produced using BET.

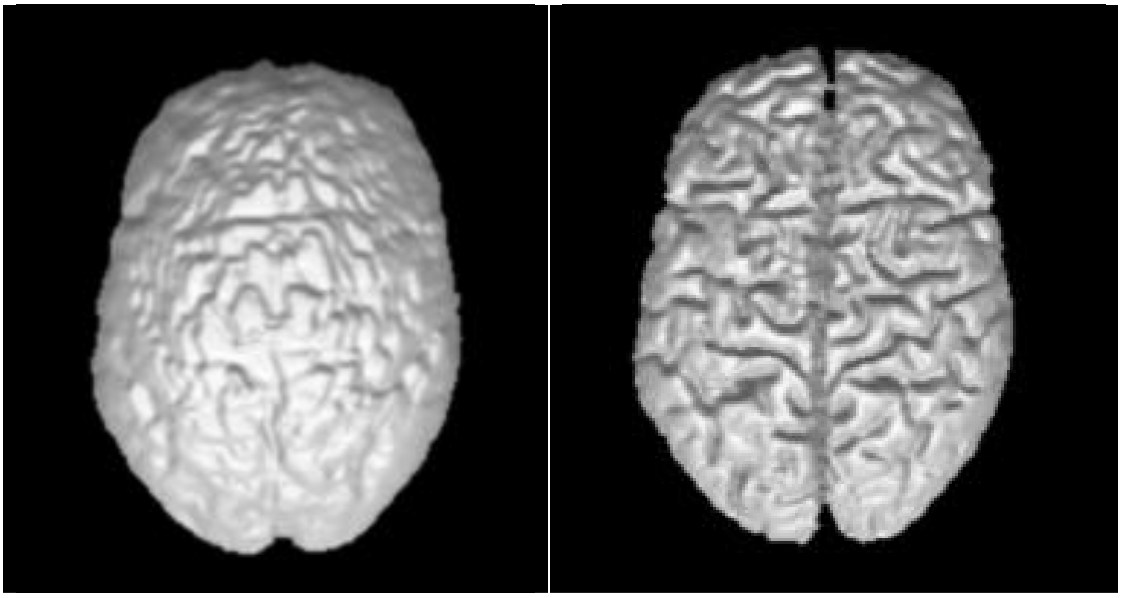

Figure 6. Example 3D rendering of a brain mask obtained using BET (left) as opposed to using our brain extraction method (right) on axial MS/MRI T1-weighted scans.

The brain extraction results of the clinical T1-weighted data in 2D are shown next (see Figure 7). BET fails to exclude the eyeballs from its brain masks, whereas our proposed method achieves better brain mask fits.

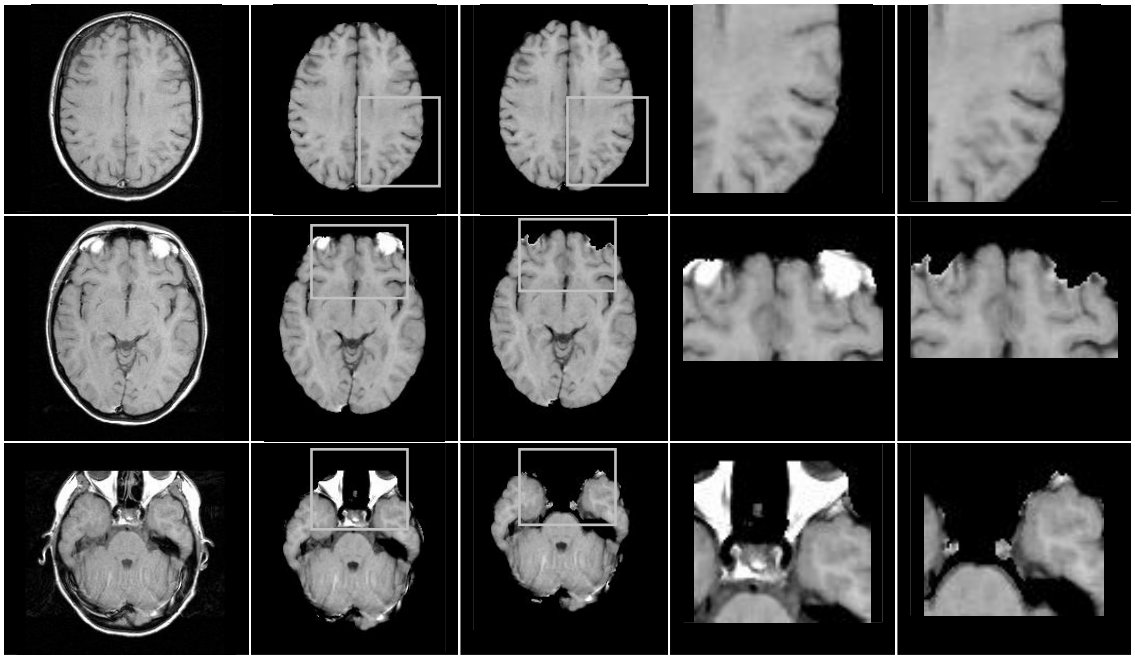

Figure 7. Axial MS/MRI T1-weighted scan, BET results, our brain extraction results, highlighted BET results, and our highlighted brain extraction results (from left to right).

5. CONCLUSIONS

We proposed a new method for extracting the brain cortex from T1-weighted MRI head scans based on techniques including Otsu's thresholding, connected component analysis, mathematical morphology, and geodesic active contours.

Our quantitative results show that the proposed method outperforms the standard BET technique with synthetic BrainWeb data, and significantly outperforms BET with real IBSR data. Our qualitative results on real clinical data against BET show that the proposed method achieves a tighter brain mask around the brain cortex with both BrainWeb and IBSR scans, and succeeds in removing problematic areas in the MS/MRI clinical scans.

REFERENCES

1. S.M. Smith, "Robust Automated Brain Extraction," *Human Brain Mapping*, vol 17, no. 3, pp. 143-155, 2002.
2. D.W. Shattuck *et al*, "Magnetic resonance image tissue classification using a partial volume model," *Neuroimage*, vol. 13, no. 5, pp. 856-876, 2001.
3. L. Lemieux *et al*, "Fast, accurate, and reproducible automatic segmentation of the brain in T1-weighted volume MRI data," *Magn Reson Med*, vol. 42, no. 1, pp. 127-135, 1999.
4. K. Rehm *et al*, "Putting our heads together: a consensus approach to brain/non-brain segmentation in T1-weighted MR volumes," *Neuroimage*, vol. 22, no. 3, pp. 1262-1270, 2004.
5. N. Otsu, "A threshold selection method from gray level histograms," *IEEE Transactions on Systems, Man and Cybernetics*, vol. 9, pp. 63–66, 1979.
6. J.G. Sled *et al*, "A non-parametric method for automatic correction of intensity non-uniformity in MRI data," *IEEE Transactions on Medical Imaging*, vol. 17, pp. 87-97, 1998.
7. P. Perona and J. Malik, "Scale-space and edge detection using anisotropic diffusion," *IEEE Transactions on Pattern Analysis Machine Intelligence*, vol. 12, pp. 629–639, 1990.
8. V. Caselles *et al*, "Geodesic active contours," *International Journal of Computer Vision (IJCV)*, vol. 22, no. 1, pp. 61–79, 1997.
9. C.A. Cocosco *et al*, "*BrainWeb: Online Interface to a 3D MRI Simulated Brain Database,"* NeuroImage, vol. 5, no. 4, part 2/4, S425, 1997 -- Proceedings of 3rd International Conference on Functional Mapping of the Human Brain, Copenhagen, May 1997.
10. R.K.-S. Kwan *et al*, *"*MRI simulation-based evaluation of image-processing and classification methods," *IEEE Transactions on Medical Imaging*, vol. 18, no. 11, pp. 1085-97, November 1999.
11. R.K.-S. Kwan, A.C. Evans, and G.B. Pike, "An Extensible MRI Simulator for Post-Processing Evaluation," *Visualization in Biomedical Computing (VBC'96)*. Lecture Notes in Computer Science, vol. 1131, pp. 135-140, Springer-Verlag, 1996.
12. D.L. Collins *et al*, "Design and Construction of a Realistic Digital Brain Phantom," *IEEE Transactions on Medical Imaging*, vol. 17, no. 3, pp. 463--468, June 1998.